Available online at www.sciencedirect.com

ScienceDirect

Current Opinion in Electrochemistry

Review Article

Porous transition metal-based nanostructures as efficient cathodes for aluminium-air batteries

Adewale K. Ipadeola[1,2], Kamel Eid[2] and Aboubakr M. Abdullah[1]

Abstract

Aluminum-air batteries (AABs) are green and efficient energy systems due to their earth-abundant, safety, low price, excellent theoretical capacity (2.98 Ah/g) and energy density (8.1 Wh/g), which are significant merits in sustainability and practical applications. However, finding an efficient electrocatalyst for oxygen-electrochemistry (i.e., OER/ORR) as an air cathode is one of the barriers to large-scale applications. Porous transition-metal-based (PTM) air cathodes are highly promising for the AABs, owing to their outstanding and tunable physicochemical properties, besides their low-cost, earth-abundance and ease of synthesis. This article emphasizes the recent advances in the fabrication of PTM air cathodes, including monometallic, bimetallic, and multimetallic, to tailor their morphologies for excellent AABs' performance. Also, a deep discussion on the challenges and current progress is anticipated for practical AABs.

Addresses

[1] Centre for Advanced Materials, Qatar University, Doha 2713, Qatar
[2] Gas Processing Center (GPC), College of Engineering, Qatar University, Doha 2713, Qatar

Corresponding authors: Ipadeola, Adewale K. (ak.ipadeola@qu.edu.qa); Abdullah, Aboubakr M. (bakr@qu.edu.qa); Eid, Kamel (kamel.eid@qu.edu.qa)

Current Opinion in Electrochemistry 2023, **37**:101198

This review comes from a themed issue on **Energy Storage: Batteries and Supercapacitors (2023)**

Edited by **Kenneth Ozoemena**

For complete overview about the section, refer Energy Storage: Batteries and Supercapacitors (2023)

Available online 16 December 2022

https://doi.org/10.1016/j.coelec.2022.101198

Keywords

Porous-transition-metals, Oxygen reduction reaction, Oxygen evolution reaction, Bifunctional electrocatalysts, Air cathodes, Aluminium-air batteries.

Introduction

The inexorable usage of non-renewable energy sources leads to huge environmental problems and climate changes [1,2], so it is urgent to find an alternative green or renewable energy. Electrochemical energy storage, including batteries [3,4] and supercapacitors [5], is an affordable, green and efficient energy system. Unlike other batteries, aluminium-air batteries (AABs) utilize preserved Al lightweight and infinite O_2 (from the air) for electricity production, because Al has practicable operating voltage, outstanding theoretical capacity and energy density, safety, earth abundance and low price (1.1-1.9 USD/kg) [6–8]. Therefore, the AABs are efficient energy systems; however, several barriers, like sluggish oxygen reduction (ORR) and evolution reactions (OER) kinetics, low performance, and high cost of noble-metal air cathodes make the AABs impracticable [6–8]. The solutions lined in developing efficient, inexpensive, high-performance and durable air cathodes using porous transition metal-based (PTM) catalysts [6–9].

The PTM materials are easily synthesized from earth abundant and inexpensive precursors with tailored morphologies (i.e., wires, rods, cubes, sheets) and endowed physicochemical features (i.e., rich active sites, conductivity, redox, porosity etc) that provide high surface area, quick charge mobility, and maximized atomic usage for ORR/OER [9]. Various synthetic approaches (i.e., hydrothermal/solvothermal, sol–gel, template-based, etc) were developed for fabricating PTMs with outstanding ORR/OER performance. Notably, PTM-electrocatalysts for ORR and OER have garnered great attention leading to nearly 12,404 and 611 published articles, respectively; however, only 58 articles reported PTM air cathodes for the AABs in the last four years, according to the Web of Science (Figure 1a). Therefore, it is significant to highlight the recent advances in this research area.

This review summarizes the recent strategies adopted for the simplistic fabrication of PTM-nanostructures, including controlled synthetic approaches and formation mechanisms, with desired morphologies for optimal air cathode performance in the AABs in the last two years (Figure 1b). Finally, AAB configuration with drawbacks and possible solutions for practical applications are discussed.

Review focus

There are several reviews on PTM-electrocatalysts for catalytic applications, like ORR and water splitting

Figure 1

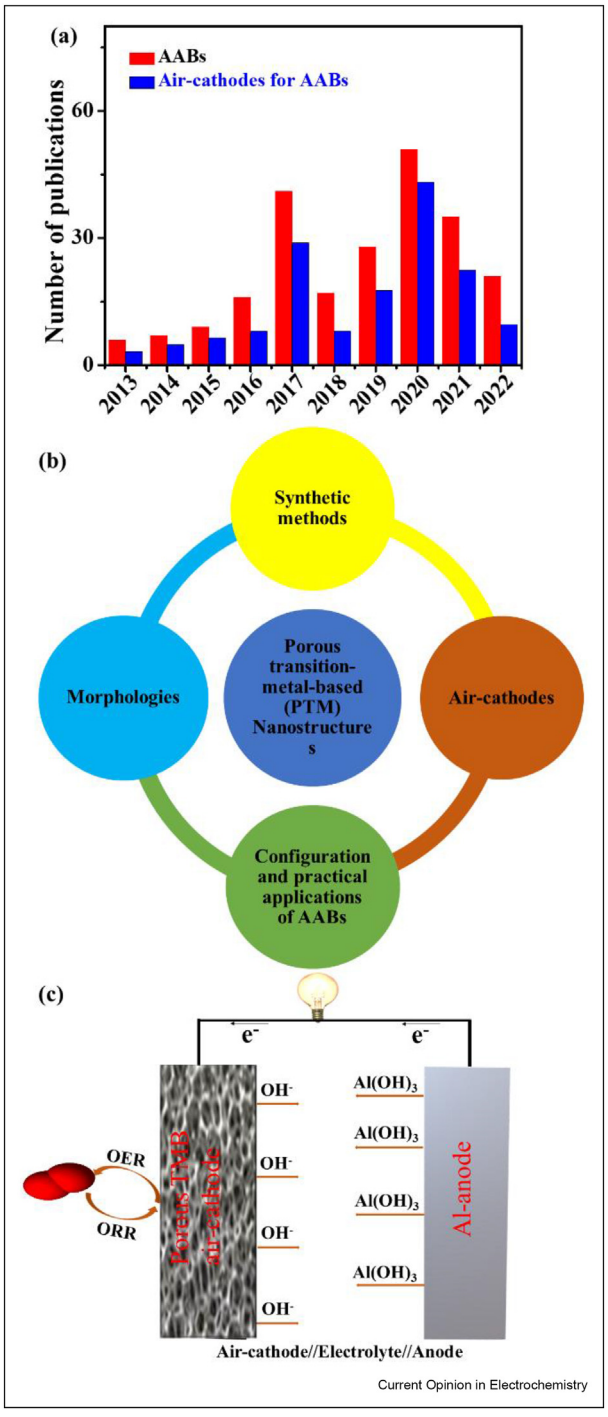

(**a**) Number of publications with keywords "aluminium-air batteries and air cathodes aluminium-air batteries" according to the Web of Science (as of August 19, 2022), (**b**) main concepts discussed and (**c**) AAB configuration.

[5,9,10], but there is no review related to AABs, as far as we found. Meanwhile, there are several challenges to the use of PTM air cathodes in the AABs, which should be highlighted and solved. This motivated us to highlight the recent advances in the controlled fabrication of PTMs-based materials as air cathode in AABs, owing to their unique physicochemical and redox properties, besides easy preparation from low-cost and earth abundant materials.

Configuration and practical applications of AABs

The AABs are mostly primary cells, comprising air cathode, electrolyte and Al-anode (Figure 1c). When the Al-anode is completely consumed by the O_2 (from air) reaction to form $Al(OH)_3$ and/or $Al(OH)_4^-$ ions in the alkaline conditions, then the generation of electricity is interrupted and the aqueous AAB becomes non-rechargeable, according to the mechanism in **Eqns (i-iii).** Continuous accumulation of $Al(OH)_4^-$ ions and consumption of OH^- ions reduce the conductivity and diffusivity of the motionless electrolyte. Hence, purification of the AAB requires the removal of the accumulated discharged products and refilling with fresh electrolytes to boost its electrical conductivity for stable and large-scale AABs. However, rechargeable AABs with a great tendency of $Al^{3+} \leftrightarrow$ Al is achieved in non-aqueous-electrolytes containing amide-groups/additives (i.e., ionic-liquid), besides mitigating Al-anode challenges. The components of AAB play complementary roles in its operation [11–14].

Cathode: $3O_2 + 6H_2O + 12e^- \rightarrow 12OH^-$ ($E^o = +0.40$ V) (i)

Anode: $4Al + 12OH\text{-} \rightarrow 4Al(OH)_3 + 12e\text{-}$ ($E^o = -2.31$ V) (ii)

Overall reaction: $4Al + 3O_2 + 6H_2O \rightarrow 4Al(OH)_3$ ($E^o = +2.71$ V) (iii)

The AAB has additional components (i.e., heat-exchanger, CO_2-scrubber and crystallizer) with robust management systems (i.e., sensors, module design and real-time software) in large-scale applications, and the viability of AABs is compared with other metal-air-batteries (Table 1) [6–8]. The performance of AABs is shaped by the electrode's efficiency and lightweight, i.e., reducing Al-weight by 1 kg increased the energy density by ~5 Wh/kg [6–8].

PTM air cathodes for AABs

Pt-based-materials remain the best air cathodes, however, their rarity and scarcity spurred the emergence of

Table 1

Comparison of AABs with other metal-air batteries based on the data in this Ref [6]. *refers to the theoretical potential for Li-ion batteries, #refers to the theoretical potential for Li-air batteries.

Metal-air batteries	Earth-abundance metal (ppm)	Theoretical SC (Ah/kg)	Theoretical energy density (kWh/kg)	Theoretical potential (V)	Price (USD/kg)	Practical operating potential (V)
Al	82,000	2980	8.13	2.71	1.9	1.2–1.6
Na	22,700	1166	2.68	2.33	3.1	1.8–2.8
Mg	23,000	2205	6.81	3.09	2.2	1.2–1.6
Zn	76	820	1.36	1.66	2.4	1.0–1.2
Li	65	3861	11.43	#2.96/*3.04	19.2	2.0–2.4

PTMs (i.e., monometallic, bimetallic and multimetallic (mainly perovskites)) as effective and low-cost air cathodes with exceptional performance [15–19], discussed below.

Mono-metallic PTM air cathodes

The monometallic-PTMs were strategically engineered on conductive materials for optimal utilization as the air cathodes [20]. Co_3O_4 nanocluster on N-doped carbon nanotubes/3D-graphene (Co_3O_4/NCNTs/3D-graphene) prepared by hydrothermal (95 °C for 10 h)/calcination (300 °C for 2 h in the air) (Figure 2a) with a formation process, including bamboo-like CNTs growth on 3D-graphene and ultrathin Co_3O_4 nanosheet wrapped around NCNTs, and utilized as air cathode (Figure 2b), which possessed hierarchical porosity, more exposed active-sites and synergism, evidenced by SEM and TEM images (Figure 2c and d) to deliver high power density (P_{max} = 4.88 mW/cm^2) and specific capacity (SC = 482.80 mAh/g_{Al}) compared to Co_3O_4/3D-graphene (4.02 mW/cm^2 and 316.59 mAh/g_{Al}) and Pt/C (361.64 mAh/g_{Al}) (Figure 2e) [21]. Similarly, reduced mesoporous Co_3O_4 nanowires grown on 3D-graphene (rm-Co_3O_4/3DG) gave high open circuit voltage (OCV = 1.53 V) and SC (422.74 mAh/gAl) than traditional m-Co_3O_4/3DG (1.51 V and 387.65 mAh/g_{Al}), m-Co_3O_4 (1.50 V and 316.59 mAh/g_{Al}) and Pt/C (1.51 V and 361.74 mAh/g_{Al}) because of its boosted charge/mass transport, surface area and defect [22]. Ultrasound-assisted hydrothermal (150 °C for 10 h) synthesis of Co_3O_4 supported N-graphene oxide (HU−Co_3O_4/N-GO) had enhanced OCV (1.20 V) than Co_3O_4/N-GO (1.18 V), owing to the fabrication mechanism of effective/uniform nucleation and growth of the Co_3O_4 cubic clusters under ultrasound with optimal nanoparticles dispersion [23]. Co-embedded NCNTs on carbon fiber paper (CoNCNT/CP) synthesized by hydrothermal (120 °C for 12 h)/carbonization (650 °C for 0.5 h in Ar) and soaked in different PTFE-solutions (0.4-1.0 wt.% for 10 min) were investigated as air cathodes [24]. 0.8-CoNCNTs/CP nanosheets morphology achieved optimal aerobic-wettability for boosted O_2-electrochemistry kinetics for superior SC (159.6 mW/cm^2) than CoNCNTs/CP (90.0 mW/cm^2). 3D-porous Cu/C-film (3DP-Cu/C-film) was synthesized by preheating at 250 °C for 1 h in Ar and then annealled at 600 °C under H_2 for 1 h and was tested as air cathode in KOH and NaOH [25]. The 3DP-Cu/C-film had excellent water-resistance and air-permeability in KOH and improved performance with high OCV, P_{max} and charge-transfer-resistance (R_{ct}) (1.31 V; 20.34 mW/cm^2 and 8.69 Ω) and long durability (>3500 s) than in NaOH (1.26 V; 12.06 mW/cm^2 and 12.72 Ω). Thus, KOH-electrolyte is more favourable for efficient air cathode. Cu_2Se nanoparticles confined in HKUST-1 (MOF-199)-derived 3D porous carbon (Cu_2Se@C) was synthesized by hydrothermal (120 °C for 12 h)/pyrolysis (600 °C for 2 h in Ar/H_2) via a fabrication process of coordination of Cu^{2+} ions and trimesic acid, and decomposition, and demonstrated as air cathode in rechargeable AAB [26]. The Cu_2Se@C exhibited unique polyhedral structures, boosted electrical conductivity, buffered volume expansion and abundant channels that enhanced Al^{3+} ions storage feature with moderate SC (276.20 mAh/g_{Al}) and discharge plateau (1.83 V).

Single-atom Fe-N_x on mesoporous carbon spheres (SA-Fe-N_x-MPCS) was fabricated by polymerization/silica-template pyrolysis (900 °C for 2 h in Ar, Figure 2f) through Fe-nucleation, co-assembled SiO_2 by electrostatic/H-bonding effects with an endowed spherical-structure, evidenced by SEM and TEM images (Figure 2g and h) that are beneficial for facile mass/charge transfer with high OCV, P_{max} and SC (1.53 V; 130 mW/cm^2 and 2204 mWh/g_{Al}) and stability (>300 h @25 mA/cm^2) comparable to Pt/C (1.54 V; 125 mW/cm^2 and 2239 mAh/g_{Al}) (Figure 2i and j) [27]. However, utilizing ferrocene and zinc-based metal−organic framework (Zn-MOF) as sacrificial templates via pyrolysis (150 °C for 2 h in Ar) for the synthesis of N-doped carbon flakes modified with Fe-single-atoms on carbon-cloth (Fe-SA-NC@CC) raised the OCV (2.1 V) with areal capacity (1.33 mW/cm^2) [28]. Fe-phthalocyanine and hollow-N,S co-doped carbon spheres (FePc@HNSCs) with π-π stacking and high dispersibility were fabricated by pyrolysis (200 °C

Figure 2

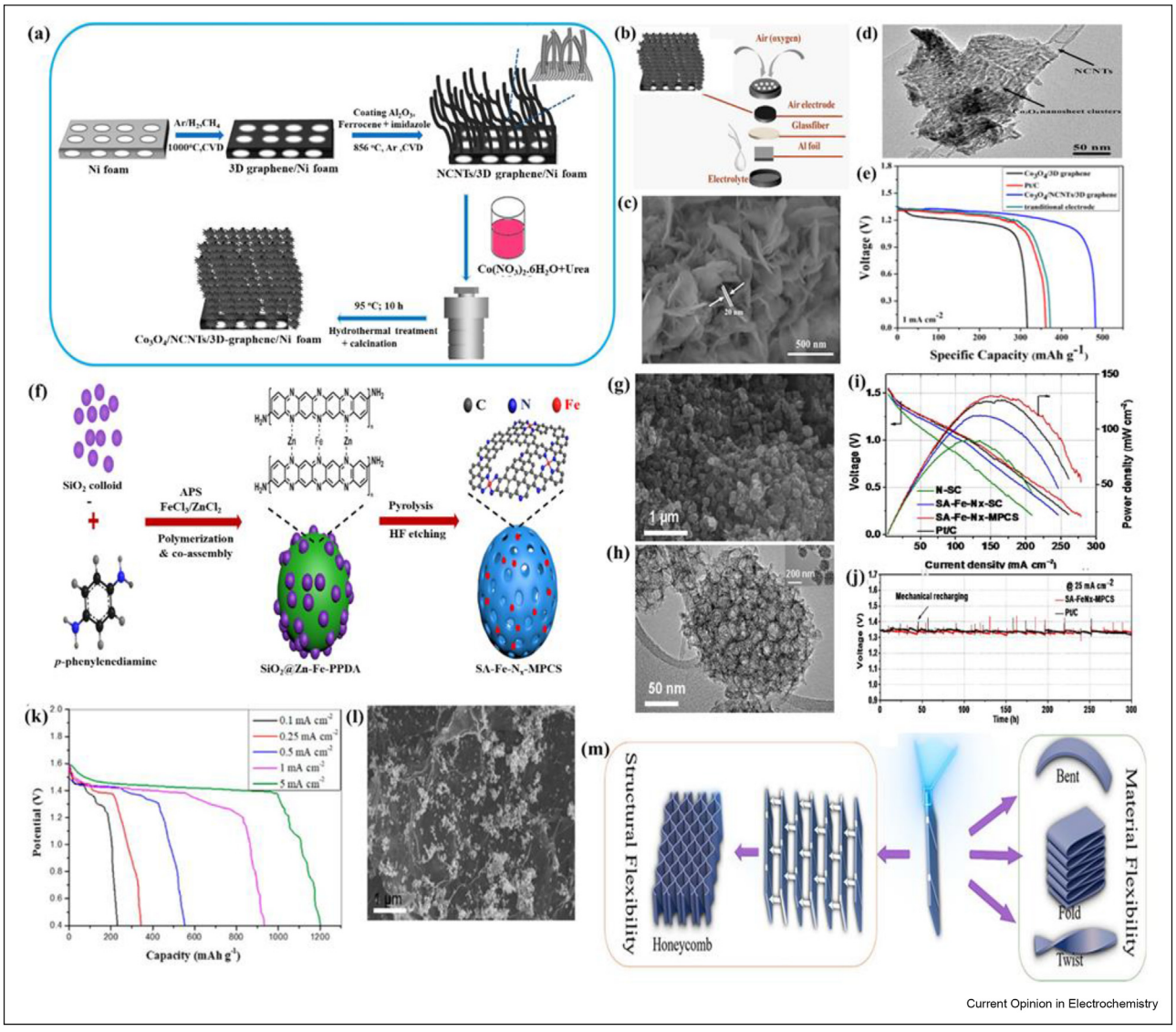

(**a**) Hydrothermal/pyrolysis synthetic scheme, (**b**) coin Al-air cell conformation, (**c**) SEM, (**d**) TEM and (**e**) specific discharge capacities of Co_3O_4/NCNTs/3D graphene and counterparts, (**f**) polymerization/pyrolysis/etching synthetic scheme, (**g**) SEM, (**h**) TEM, (**i**) voltage–power curves and (**j**) stability of SA-FE-Nx-MPCS. Copyright 2020,2021 Elsevier [21,27]. (**k**) galvanostatic discharge at 5 mA/cm^2 and below, (**l**) SEM and (**m**) Conceptual illustration of honeycomb-like stretchable AABs using γ-MnO_2-N/S graphene air cathode. Copyright 2020 American Chemical Society [32].

for 2 h in Ar) and tested as air cathode, exhibited increased electron density on Fe−N_4, up-shifted Fe d-band and synergism for superior OCV, P_{max} and SC (∼1.92 V; 204.7 mW/cm^2 and 1320 mWh/g_{Al}) than Pt/C (∼1.83 V; 184.3 mW/cm^2 and 1252 mAh/g_{Al}) [29].

Grinding of MnO_2 nanoparticles with carbon black Vulcan/carbon cloth (MnO_2-CB/CC) gave a promising air cathode with good OCV; P_{max} and R_{ct} (1.4 V; ∼28 mW/cm^2 and 1.3 Ω) relative to CB/CC (∼1.39 V; ∼20 mW/cm^2 and 13.7 Ω) [30]. Thus, the addition of MnO_2 to CB/CC facilitated electron transport for boosted air cathode. However, the utilization of hydrothermally (90 °C for 4 h) synthesized Mn_3O_4/graphene gave a low OCV (1.17 V), but high R_{ct} (2.88 Ω) [31]. This was plausibly due to the instability of Mn^{3+}, according to the Jahn-Taller effect, with fluctuating Mn^{3+}/Mn^{4+} ratio, a drawback for Mn_3O_4, hence, MnO_2 is often explored. γ-MnO_2-N/S-graphene prepared by hydrothermal (140 °C for 2 h) displayed an excellent SC (1203.2 mAh/g_{Al} @5 mA/cm^2, Figure 2k), due to its nanorod structures (SEM, Figure 2l) with high surface area, porosity and conductivity for facile O_2 diffusion and transport in an advanced honeycomb-shaped

stretchable AABs (Figure 2m) [32]. Similarly, γ-MnO_2 nanorod assembled hierarchical microspheres prepared by calcination (250−350 °C for 2 h in Ar) delivered superb OCV and P_{max} (1.85 V and 318 mW/cm^2) compared to pristine-γ-MnO_2 (1.64 V and 176 mW/cm^2) [33]. This was attributed to the optimized O_2 vacancies. Hydrothermal (180 °C for 10 h)/annealing (900 °C for 3 h in N_2)/plasma-surface-etching (1−4 min) methods were explored to prepare O/N co-doped carbon nanofiber anchored MnO/Mn_2O_3 (MnO/Mn_2O_3/ONCNF) and demonstrated as air cathode [34]. The etching process endowed MnO/Mn_2O_3/ONCNF-3 nanofiber with a strong synergy of O/N/Mn^{2+}/Mn^{3+} ions and rich-defect to deliver P_{max} (129.7 mW/cm^2) comparable to Pt/C (136.2 mW/cm^2).

Bimetallic-PTM-air-cathodes

Combing two transition metals as air cathodes is one of the effective approaches to augmenting physicochemical features advantageous for O_2 electrocatalysis [4,35,36]. Intercalation of Co-ions into MnO_2/C at different mole ratios (x%Co−MnO_2/C, x = 0−50) by hydrothermal (70 °C for 1 h), via electrostatic interaction, where 40% Co−MnO_2/C displayed an impressive air cathode with OCV (1.80 V) and SC (375 mAh/gAl) in rechargeable AABs compared to other compositions, due to its optimized active sites and O_2 transport channels [37]. Similarly, Co_2O_3 nanorod embedded α-MnO_2 (α-MnO_2/Co_3O_4) by hydrothermal (140 °C for 12 h)/pyrolysis (400 °C for 4 h) possessed a porous structure with a large surface area that gave a more stable discharge SC (250 mAh/g_{Al}) [38]. The addition of urea/amide to the electrolyte facilitated the rechargeability of $Al(OH)_3$/$Al(OH)_4^-$, but with lower SC than the primary AAB. A series of $NiMn_2O_4$ (Ni−Mn) was fabricated by hydrothermal (130 °C for 10 h)/calcination (600−900 °C for 12 h in the air) (Figure 3a) and tested as air cathodes in KOH−Na_2SnO_3−ZnO−$In(OH)_3$ electrolyte [39]. Ni-Mn-600 possessed high (Mn^{3+}+Mn^{4+})/$Mn^{2+}$and Ni^{3+}/Ni^{2+}-ions) with nanorod morphology, proved by SEM image (Figure 3b) for superior air cathode with high OCV, P_{max} and SC (1.72 V; 100.45 mW/cm^2 and 2626.1 mAh/g_{Al}) than Ni−Mn-900 (1.28 V; 2060.2 mAh/g_{Al}) but comparable to Pt/C (1.83 V; 76.10 mW/cm^2 and 2719.3 mAh/g_{Al}) (Figure 3c and d). CeO_2 nanoparticles embellished MnOOH nanorod (MnOOH@CeO_2) synthesized by solvothermal (120 °C for 12 h) was investigated as air cathode [40]. The formation mechanism of MnOOH@CeO_2 involved reduction, precipitation, hydrolysis and attachment of CeO_2 to MnOOH to ensure nanorod structures that delivered superior P_{max} and SC (302.80 mW/cm^2 and 2762.80 mAh/g_{Al}) than Pt/C (20 wt.% Pt) (257.7 mW/cm^2 and 2483.5 mAh/g_{Al}) (Figure 3e), due to the strong synergy of MnOOH@-CeO_2 for facile O_2 activation/enrichment (Figure 3f) and H_2O_2 inhibition. Atomically-dispersed-Fe/Co-moieties on NCNT (f-FeCo-NC) at varied Fe^{2+}+Co^{2+} molar ratio (10−15%) by solvothermal (190 °C for 6 h)/carbonization (900 °C for 1 h in N_2) via fabrication process of metal dispersion in formamide and immobilization of Fe/Co-sites at high-temperature were tested as air cathode [41]. f-FeCo−NC−12 (at a ratio of 12%) gave the most active sites, electron/ionic conductivity and surface area that enabled high P_{max} (188.8 mW/cm^2) than Pt/C (176.7 mW/cm^2). The ultrasound-assisted ion-exchange method was employed to prepare an electronically engineered amorphous Fe-Co-S-sites embedded in Prussian blue analogue ($FeCoS_x$-PBA) and studied experimentally and theoretically as an air cathode in a flexible AAB [42]. This study revealed that the encapsulation of Fe-Co-S_x into PBA significantly improved the electron transfer with hollow hetero-nanoframe morphology that suppressed OH overbinding but moderately increased its cathodic performance with P_{max} (58.30 mW/cm^2), SC (1483 Wh/kg_{Al}) and excellent durability (>50 h).

CoNi nanoalloy confined N-doped carbon framework (CoNi-NCF) synthesized by sol−gel/pyrolysis (900 °C for 2 h in N_2) of Ni-ZIF67@SiO_2 template to stabilize NCF, coalescence CoNi and then SiO_2 removal, utilized as air cathode in NaOH and NaCl [43]. Facile O_2 adsorption and desorption on CoNi-NCF were proven by the density functional theory (DFT, Figure 3g and h), besides abundant dual active-sites (Co^{III}/Ni^{III}), rhombic-dodecahedral structures (Figure 3i) and porosity (Figure 3j) of NCF-matrix facilitated high P_{max} (203.69 and 21.50 mW/cm^2) and durability in NaOH and NaCl than Pt/C (180.72 and 19.06 mW/cm^2), respectively. CoNi alloys were rationally grown on intertwined N-doped carbon nanotube arrays onto CC substrates (CoNi@NCNTs/CC) was achieved via hydrothermal (120 °C for 6 h)/calcination (800 °C for 3 h in N_2) through the fabrication mechanism of CoNi nanoparticles growth on CC by the reducing gases produced from the C_3N_4 decomposition, and was assembled as air cathode in liquid- and solid-state AABs [44]. The CoNi@NCNTs/CC exhibited high air cathodic performance with OCV (1.68 and 1.61 V), P_{max} (151 and 91 mW/cm^2), SC (1029.00 mAh/g) and energy density (1399 Wh/kg), due to its nanotube clusters with abundant active sites, optimized adsorption energy, large surface area and rapid mass transfer. NiCo selenide anchored into fluorine-doped carbon ($NiCoSe_2$@F−C) was prepared by solvothermal (200 °C for 10 h)/annealing (600 °C for 2 h in Ar) using polyvinylidene fluoride (PVDF) as dopant/structure directing agent and tested as air cathode for rechargeable AAB [45]. The $NiCoSe_2$@F−C has nanospheres/core−shell structures abundant mesoporous, nanosize and high surface area that facilitated fast $AlCl_4^-$ ions intercalation/deintercalation to deliver high reversible SC (294.00 mAh/g_{Al}) and stable coulombic efficiency (98%).

Figure 3

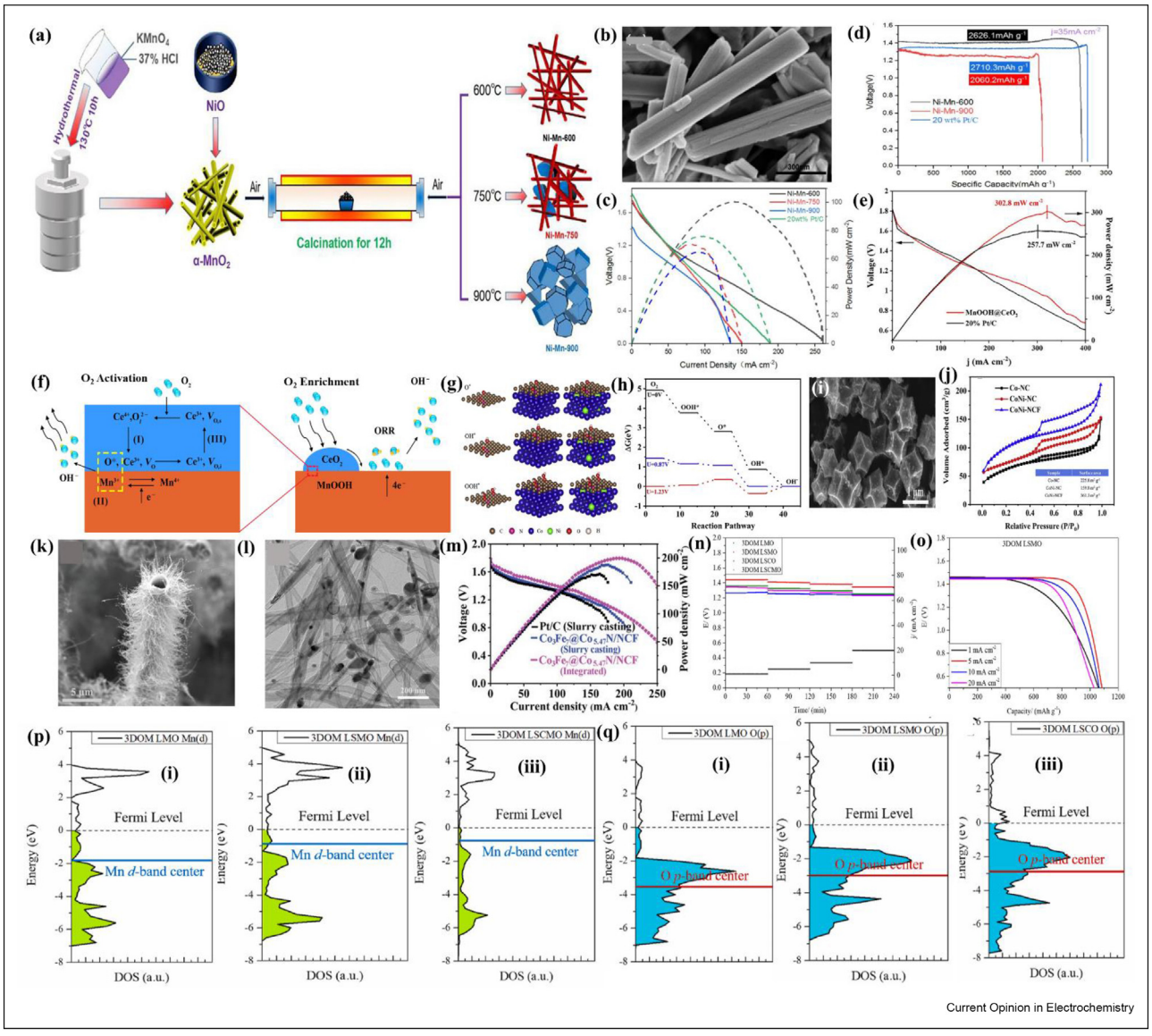

(**a**) Hydrothermal/calcination synthetic scheme, (**b**) SEM, (**c**) polarization-power density curves and (**d**) specific capacity of Ni−Mn-600 and counterparts. (**e**) Power density curves and (**f**) illustrative synergistic effect of MnOOH−CeO_2 toward O_2 reactions, (**g**) optimized structures of adsorbates (OH*, O* and OOH*), (**h**) the free-energy landscape of the adsorbates in $4e^-$ mechanism during O_2 reactions, (**i**) SEM and (**j**) N_2 adsorption−desorption isotherms of CoNi-NCF and counterparts. Copyright 2020,2021 Elsevier [39,40,43]. (**k**) SEM, (**l**) TEM and (**m**) discharge polarization-power curves of Co_3Fe_7@$Co_{5.47}$N/NCF integrated and slurring coating air cathodes. Copyright 2020 Wiley-VCH [47]. (**n**) galvanostatic discharge for 240 min, (**o**) specific capacity at different current densities, (**p**) PDOS diagram and O p-band centres relative to the Fermi surface of (i) LMO, (ii) LSMO and (iii) LSCO. Copyright 2022 Elsevier [52].

The construction of Co_3Fe_7−Fe_3C on honeycomb-N-carbon (Co_3Fe_7−Fe_3C/HNC) from biomass oxidation/pyrolysis (900 °C for 2 h in N_2) using K_2FeO_4 as Fe precursor/oxidizing agent for lignocellulose cross-linking and Co/N trapped from soybean roots afforded 3D honeycomb structures, and exhibited as air cathode with P_{max} (210 mW/cm^2) than Pt/C (180 mW/cm^2), owing to the controlled heterostructures with charge transfer close to an ideal-catalyst [46]. Indeed, interfacial engineering is an excellent approach for improving air cathode performance. Comparative Co_3Fe_7@$Co_{5.47}$N on N-doped carbon foam (Co_3Fe_7@$Co_{5.47}$N/NCF) assembled as slurry-casting and integrated air cathodes [47]. The integrated-Co_3Fe_7@$Co_{5.47}$N/NCF took advantage of its uniform nanoparticles dispersion on dandelion/3D-hollow-structure, evidenced by SEM and TEM images (Figure 3k and l), with fast electron/mass transfer and binder-free flexibility for high P_{max} and SC

(199.6 mW/cm^2 and 1997.3 mAh/g_{Al}) than slurry-casting-Co_3Fe_7@$Co_{5.47}$N/NCF (187.7 mW/cm^2 and 1911.3 mAh/g_{Al}) and Pt/C (171.3 mW/cm^2 and 1773.9 mAh/g_{Al}) (Figure 3m). Single-atoms Fe-Ni were dispersed on N-doped-carbon (FeNi SAs/NC) via polydopamine (PDA) coating spatial-confined pyrolysis and etching that resulted in hollow cube morphology with more exposed FeNi-dual-sites for high OCV, P_{max} and SC (1.87 V; 52.12 mW/cm^2 and 1576.4 mAh/g_{Al}) and operating voltage after 5 h compared to Pt/C (1.83 V; 45.25 mW/cm^2 and 1498.6 mAh/g_{Al}) [48]. Novel Fe-doped Nickel selenide (Fe−NiSe) was synthesized by hydrothermal (120 °C for 8 h)/annealing (600 °C for 2 h in Ar) and examined as air cathode for rechargeable AAB [49]. The Fe−NiSe possessed microflower with ultrafine nanostructures, multiple active sites and rapid ions diffusion that enabled $AlCl_4^-$ ions intercalation/de-intercalation to deliver remarkable SC (304.00 mAh/g_{Al}), energy density (402.50 Wh/kg) and excellent cycling stability (13,500 cycles). This study proved that a strong synergy between ultrafine nanostructure and heteroatom doping is an efficient strategy for boosting the durability and high energy of AABs.

The fabrication of Fe/CoP_2 embedded wheat-straw-carbon (FeCoP_2-NPWC) was prepared via the activation/pyrolysis at 1000 °C for 2 h in Ar/H_2 and then utilized as air cathode in liquid and solid AABs. FeCoP_2-NPWC gave an excellent P_{max} and SC (87.1/43.2 mW/cm^2 and 1212 mAh/g_{Al}) relative to Pt/C−RuO_2 (62.6/23.9 mW/cm^2 and 987 mAh/g_{Al}), owing to its unique layered shell structure and synergism [50]. The DFT calculations of energy barriers of single-atom Cu incorporated Fe−N−C aerogels (NCAG/Fe−Cu) revealed low magnetic moment, altered Fe 3 d-electrons, Fe−Cu heteronuclear dual-sites and honeycomb-like morphology that boosted its air cathode in neutral and quasi-solid (PANa) electrolytes with superior OCV and P_{max} (2.0 V and 130 mW/cm^2) than Pt/C (1.82 V and 96 mW/cm^2) [51].

Multi-metallic PTM air cathodes

Porous perovskite-oxides are the most recently explored multimetallic PTM air cathodes in AABs because of their distinct physicochemical features for excellent electrocatalysis [9,53]. Three distinct $La_{0.7}Sr_{0.3}MnO_3$(LSMOs) were prepared by SiO_2-template pyrolysis/etching, template-free pyrolysis and sol−gel methods and investigated as air cathodes [54]. The SiO_2-templated-LSMO had increased specific surface area and 2D-porosity that facilitated its remarkable OCV, SC and energy density (1.46 V; 1048.6 mAh/g_{Al} and 1020.6 mWh/g) compared to template-free-LSMO (1.41 V; 961.9 mAh/g_{Al} and 934.7 mWh/g) and sol−gel-LSMO (1.27 V; 659.7 mAh/g_{Al} and 688.6 mWh/g). $La_{0.4}Sr_{0.6}Co_{0.7}FeNb_{0.1}O_{3-\delta}$ synthesized by sol−gel/pyrolysis (LSCFN-SG, 700 °C for 3 h) and conventional solid-phase (LSCFN-SP, 1050 °C for 5 h) methods were comparatively studied as air cathodes [55]. The study showed that the metals' oxidation states were altered by the sol−gel method and enabled LSCFN-SG with increased surface area, mesoporous structures and more active sites (Co^{3+}/Co^{2+} ratio) for effective O_2 diffusion and kinetics to deliver high P_{max} (68 mW/cm^2) than LSCFN-SP (56 mW/cm^2). Different 3D-ordered mesoporous perovskites with A/B-sites elements, comprising 3DOM-LSMO, 3DOM-LSCO and 3DOM-LSCMO were prepared by hydrothermal (100 °C for 12 h)/calcination (300 °C for 3 h in N_2; 700 °C for 4 h in air) methods and examined as air cathodes [52]. The 3DOM LSMO exhibited great air cathode activity with SC (1084 mAh/g_{Al}) and long durability (>240 min) (Figure 3n and o), attributable to the ideal Mn valence-state and d-band-center (0.82 eV), proved by the partial density of states (PDOS, Figure 3p and q), high surface area and porosity with more exposed three-phase interface and active-sites. The key parameter indicators for PTM air cathodes in AABs are highlighted (Table 2).

Conclusion and prospects

This review summarizes the recent advances in PTMs (i.e., monometallic, bimetallic, and multi-metallic) nanostructures as air cathodes for the AABs. This includes relationships between their synthetic processes, morphologies and performance as air cathodes for AABs in the past two years. Deep discussion and analysis of the PTM air cathodes' performance and their current challenges are presented. The PTMs were prepared with varied morphologies, including 0D (i.e., dots, spheres), 1D (i.e., fiber, rods, tubes, wires), 2D (i.e., sheets, flakes), 3D (i.e., honeycomb, dandelion-like) and polyhedron (i.e., rhombic, cubes, hexagonal), and gave wide-ranging electrochemical activities. This is based on various preparation methods (i.e., template-based, sol−gel, pyrolysis/etching, solvothermal/hydrothermal, and ultrasonic-assisted). In this report, Fe-SA-NC@CC showed the highest OCV (2.1 V), due to the coupling effect of Fe single-atom with MOF-derived-NC and carbon-support [28]. Also, NCAG/Fe−Cuhoneycomb [51], Co_3Fe_7−Fe_3C/HNC honeycomb [46], FePc@HNSC hollow-sphere [29], and Co_3Fe_7@$Co_{5.47}$N/NCF [47] are promising with OCV and P_{max} (2.0 V and 137.00 mW/cm^2; 2.0 V and 210 mW/cm^2; 1.92 V and 204.70 mW/cm^2; and 1.80 V and 100.60 mW/cm^2), respectively. The highest SC (2762.80, 2626.10 and 2204.0 mAh/g_{Al}) are reported for MnOOH@CeO_2 nanorods [40], Ni−Mn-600 nanorods [39] and SA-Fe-N_x-MPCS mesoporous-spheres [27], respectively. This indicates that 1D-nanostructures are most preferred in delivering excellent OCV, P_{max} and SC, due to the accessibility of interior/exterior active sites, high surface area, and well-dispersion of single-atoms. KOH, NaOH with or without additives (like

Table 2

Summary of the porous PTM air cathodes in AABs with regards to morphologies, synthesis methods, electrolytes, open circuit voltage (OCV) and specific capacity (SC).

Air-cathodes	Morphology	Synthesis methods	Electrolytes; Anode	OCV (V)/P_{max} (mW/cm^2)	SC (mAh/g_{Al})	Ref.
Co_3O_4/NCNTs/3D graphene	Nanosheets	Hydrothermal/calcination	2 M KOH; Al foil	1.52/4.88	482.80	[21]
rm-Co_3O_4/3D graphene	Nanowires	Hydrothermal/Thermal	4 M KOH; Al-foil	1.53/-	422.74	[22]
HU-Co_3O_4/N-GO	Cubic clusters	Ultrasonic-assisted hydrothermal	4 M KOH; Pure Al	1.02/-	–	[23]
0.8-CoNCNTs/CP	Nanosheets arrays	Hydrothermal/carbonization	6 M KOH; Al foil	1.79/159.60	–	[24]
3DP-Cu/C-film	3D porous	Heat treatment	1 M KOH; Al foil	1.31/20.34	–	[25]
Cu_2Se@C	Polyhedral	Hydrothermal/annealing	$AlCl_3$-[EMIm]Cl; Al foil	-/-	276.20	[26]
SA-Fe-N_x-MPCS	Mesoporous spherical	Polymerization/pyrolysis	6 M KOH/10 mM Na_2SnO_3/ 7.5 mM ZnO/0.5 mM $In(OH)_3$; Al foil	1.53/130.00	2204.00	[27]
Fe-SA-NC@CC	Sheet-like	Template pyrolysis	6 M KOH/10 mM Na_2SnO_3/ 7.5 mM ZnO/0.5 mM $In(OH)_3$; Al foil	~2.10/3.94	1.33 mW/cm^2	[28]
FePc@HNSC	Hollow- spherical	Exfoliate/carbonization	6 M KOH/10 mM Na_2SnO_3/ 7.5 mM ZnO/0.5 mM $In(OH)_3$; Al alloy plate	~1.92/204.70	1320.00	[29]
MnO_2-CB/CC	Fibers	Mixture grinding	2 M KOH; Al plate	~1.40/28.00	–	[30]
Mn_3O_4/graphene	Hexagonal sheet	Hydrothermal	0.05 wt% PSS/ graphene + 4 M NaOH; pure-Al	1.17/-	–	[31]
γ-MnO_2-N/S graphene	Nanorod-like	Hydrothermal	PVA-PEO-KOH-casein-Na_2SnO_3;Al-foil	~1.10/2.01	1203.20	[32]
300°C-Ar γ-MnO_2	Nanorods	Hydrothermal/calcination	4 M KOH; Al foil	1.85/318.00	–	[33]
MnO/Mn_2O_3/ONCNF-3	Nanofiber	Plasm surface etching/ annealing	4 M NaOH; Al–Mg–Sn alloy	1.80/129.70	–	[34]
40%Co–MnO_2/C	Laminated sheets	Redox	$AlCl_3$-urea ionic liquid; Al sheet	1.80/-	375.00	[37]
α-MnO_2/Co_3O_4	Nanorods	Hydrothermal/pyrolysis	$AlCl_3$-[EMIm]Cl; Al-sheet	~1.50/-	250.00	[38]
Ni–Mn-600	Nanorods	Hydrothermal/calcination	6 M KOH; Al foil	1.72/100.45	2626.10	[39]
MnOOH@CeO_2	Nanorods	Solvothermal	6 M KOH-10 M Na_2SnO_3-7.5 mM ZnO-0.5 mM $In(OH)_3$; Al plate	1.80/302.80	2762.80	[40]

f-FeCo−NC−12	Bright dots	Solvothermal/pyrolysis	6 M KOH-10 M Na_2SnO_3-7.5 mM ZnO-0.5 mM $In(OH)_3$; Al foil	1.89/188.80	–	[41]
$FeCoS_x$-PBA	Nanocubes	Ultrasound-assisted ion-exchange	2 M KOH-10 M Na_2SnO_3-PVA-7.5 mM ZnO-0.5 mM $In(OH)_3$; Al foil	1.30/58.30	1259.00	[42]
CoNi-NCF	Rhombic dodecahedral	Sol−gel/Pyrolysis/etching	4 M NaOH; Al−Mg−Sn alloy	~1.95/203.69	–	[43]
CoNi@NCNTs/CC	Nanotube clusters	Hydrothermal/Pyrolysis	6 M KOH-10 M Na_2SnO_3-7.5 mM ZnO-0.5 mM $In(OH)_3$; Al plate	1.68/151.00	1029.00	[44]
$NiCoSe_2$@F−C	Nanosphere/core−shell	Solvothermal/pyrolysis	$AlCl_3$/[EMIm]Cl; Al foil	-/-	294.00	[45]
Co_3Fe_7−Fe_3C/HNC	Honeycomb-like	Impregnation/pyrolysis	4 M KOH; Al−Mn−Sn alloy	~2.00/210.00	–	[46]
Co_3Fe_7@$Co_{5.47}N$/NCF	Dandelion/3D hollow network	Impregnation/pyrolysis	1 g PVA-18 M KOH-20 mM Zn acetate; Al−Mg−Sn alloy	~1.80/199.60	1997.30	[47]
FeNi SAs/NC	Hollow-cubes	Annealing/etching	Acrylic acid-8.4 M KOH-10 mM Na_2SnO_3-7.5 mM ZnO-0.5 mM $In(OH)_3$−15 mM $K_2S_2O_8$; Al foil	1.87/52.12	1576.40	[48]
Fe−NiSe	Nanoflakes	Hydrothermal/pyrolysis	$AlCl_3$/[EMIm]Cl; Al-foil	1.80/-	304.00	[49]
$FeCoP_2$-NPWC	Layered shell	Activation/Pyrolysis	6 M KOH-10 mM Na_2SnO_3-7.5 mM ZnO-0.5 mM $In(OH)_3$; Al sheet	1.52/87.10	1212.00	[50]
NCAG/Fe−Cu	Honeycomb-like	Pyrolysis/etching	PANa-10 wt.% NaCl; Al plate	2.00/137.00	–	[51]
$La_{0.7}Sr_{0.3}MnO_3$	3D Spherical	Template	Acrylamide hydrogel	1.46/6.50	1048.60	[54]
LSCFN-SG	Mesoporous	Sol−gel/calcination	4 M KOH; $Al(OH)_6$ alloy	1.70/68.00	–	[55]
3DOM LSMO	3D microspheres	Template pyrolysis	Polyacrylamide hydrogel; Al foil	1.41/3.24	1084.00	[52]

Na_2SnO_3–ZnO–$In(OH)_3$, PVA-PEO-casein, ionic liquid, acrylic-cid-Na_2SnO_3–ZnO–$In(OH)_3$–$K_2S_2O_8$, PANa-10 wt.% NaCl, acrylamide-hydrogel, and polyacrylamide-hydrogel) are the main electrolytes used in AABs to further boost its performance, rechargeability and circumventing Al-anode corrosion. Although there are significant achievements in the exploration of PTM air cathodes for AABs, various fences are still precluding the practical utilization, so the current drawbacks should be addressed:

- ➢ The template-based method is the most promising for controlling the porosity and surface area of PTMs; however, it requires multiple-reaction steps and hazardous chemicals to etch the template and give a low yield. The development of a facile and template-free approach with high yield and well-dispersed atomic metal rather than bulk is needed to meet large-scale requirements.
- ➢ Using carbon supports for PTMs is essential to enhance conductivity and charge mobility, however, de-attachment/aggregation are crucial issues, which could be solved via the direct fabrication of PTMs over carbon-based supports.
- ➢ The simulation studies can be used with experimental studies to predict the performance and optimize the parameters as a function of preparation, morphologies, and compositions besides deciphering reaction mechanisms. Using in-situ characterization tools is essential to understand the reaction mechanisms and sort out the effect of various parameters (i.e., electrolyte, additives, corrosion, catalyst shape, and intermediates) on the performance of AABs.
- ➢ PTMs are currently used in aqueous and non-aqueous/gel/solid-state electrolytes with or without additives for AABs. However, the self-discharge of aqueous electrolytes and inferior conductivity of non-aqueous electrolytes require using additives, whose effect on the mechanism is ambiguous and should be elaborated. Gel/solid-state electrolytes are promising for the fabrication of flexible/portable Al-air cells, but their lower conductivity and mechanical properties should be improved.
- ➢ Future directions should focus on boosting the performance of AABs via alloying the Al-anode with metals (i.e., Ti, Sn, Zn) and defects engineering. Also, Al-nanostructures instead of microstructures have better physicochemistry (i.e., surface area, active sites, quantum effect). The energy cycling efficiency can also be improved by purifying/refining Al-anode, which should be most important for the commercialization of AABs in the future. The cost of AABs could be decreased significantly when Al-anode is entirely recycled through the industrial primary Al-reduction process. Mainly using commercial purified Al ($\sim 2.9\ \$\cdot kg^{-1}$) instead of pure Al ($\sim 30\ \$\cdot kg^{-1}$) could decrease the cost by 90%.
- ➢ There is an urgent need for a global protocol to evaluate the AABs, including the electrolyte concentration, volume, stability and electrode areas.

Declaration of competing interest

The authors declare that they have no known competing financial interests or personal relationships that could have appeared to influence the work reported in this paper.

Data availability

No data was used for the research described in the article.

Acknowledgement

This work was supported by (i) the Qatar National Research Fund (QNRF, a member of the Qatar Foundation) through a National Priority Research Program Grant (NPRP13S-0117-200095) and (ii) Qatar University through a High-Impact Grant (QUHI-CAM-22/23–550).

References

Papers of particular interest, published within the period of review, have been highlighted as:

* of special interest
** of outstanding interest

1. Eid K, Lu Q, Abdel-Azeim S, Soliman A, Abdullah AM, Abdelgwad AM, Forbes RP, Ozoemena KI, Varma RS, Shibl MF: **Highly exfoliated $Ti_3C_2T_x$ MXene nanosheets atomically doped with Cu for efficient electrochemical CO_2 reduction: an experimental and theoretical study**. *J Mater Chem* 2022, **10**: 1965–1975.

2. Eid K, Sliem MH, Al-Ejji M, Abdullah AM, Harfouche M, Varma RS: **Hierarchical porous carbon nitride-crumpled nanosheet-embedded copper single atoms: an efficient catalyst for carbon monoxide oxidation**. *ACS Appl Mater Interfaces* 2022, **14**:40749–40760.

3. Peng Q, Rehman J, Eid K, Alofi A, Laref A, Albaqami M, Alotabi R, Shibl M: **Vanadium carbide (V_4C_3) MXene as an efficient anode for Li-ion and Na-ion batteries**. *Nanomaterials* 2022, **12**:2825.

4. Ipadeola AK, Haruna AB, Gaolatlhe L, Lebechi AK, Meng J, Pang Q, Eid K, Abdullah AM, Ozoemena KI: **Efforts at enhancing bifunctional electrocatalysis and related events for rechargeable zinc-air batteries**. *Chemelectrochem* 2021, **8**: 3998–4018.

5. Rehman J, Eid K, Ali R, Fan X, Murtaza G, Faizan M, Laref A, Zheng W, Varma RS: **Engineering of transition metal sulfide nanostructures as efficient electrodes for high-performance supercapacitors**. *ACS Appl Energy Mater* 2022, **5**:6481–6498.

6. Liu X, Jiao H, Wang M, Song W-l, Xue J, Jiao S: **Current progresses and future prospects on aluminium–air batteries**. *Int Mater Rev* 2021, **67**:734–764.

7. Ryu J, Park M, Cho J: **Advanced technologies for high-energy aluminum–air batteries**. *Adv Mater* 2019, **31**, 1804784.

8. Liu Y, Sun Q, Li W, Adair KR, Li J, Sun X: **A comprehensive review on recent progress in aluminum–air batteries**. *Green Energy Environ* 2017, **2**:246–277.

9. Lebechi AK, Ipadeola AK, Eid K, Abdullah AM, Ozoemena KI: **Porous spinel-type transition metal oxide nanostructures as emergent electrocatalysts for oxygen reduction reactions**. *Nanoscale* 2022, **14**:10717–10737.

10. Pan J, Tian XL, Zaman S, Dong Z, Liu H, Park HS, Xia BY: **Recent progress on transition metal oxides as bifunctional**

catalysts for lithium-air and zinc-air batteries. *Batteries Supercaps* 2019, **2**:336–347.

11. Lv C, Zhang Q, Zhang Y, Yang Z, Wu P, Huang D, Li H, Wang H, Tang Y: **Synergistic regulating the aluminum corrosion by ellagic acid and sodium stannate hybrid additives for advanced aluminum-air battery**. *Electrochim Acta* 2022, **417**, 140311.

12. Xie Y, Meng X, Qin Z, Chang Y, Mao D, Wan L, Huang Y: **Reversible passivation in primary aluminum-air batteries via composite anodes**. *Energy Storage Mater* 2022, **49**:537–545.

13. Xie Y, Meng X, Mao D, Chang Y, Wan L, Huang Y: **Deformation-driven modification of Al-Li-Mg-Zn-Cu high-alloy aluminum as anodes for primary aluminum-air batteries**. *Scripta Mater* 2021, **212**, 114551.

14. Wang L, Cheng R, Liu C, Ma M, Wang W, Yang G, Leung M, Liu F, Feng S: **Trielectrolyte aluminum-air cell with high stability and voltage beyond 2.2 V**. *Mater Today Phys* 2020, **14**, 100242.

15. Ipadeola AK, Mwonga PV, Ozoemena KI: **Hydrogen oxidation and oxygen reduction reactions on palladium nano-electrocatalyst supported on nickel-deficient MOF-derived carbons**. *Electrochim Acta* 2021, **390**, 138860.

16. Ipadeola AK, Mwonga PV, Ray SC, Maphanga RR, Ozoemena KI: **Bifunctional behavior of Pd/Ni nanocatalysts on MOF-derived carbons for alkaline water-splitting**. *Electroanalysis* 2020, **32**:3060–3074.

17. Mwonga PV, Ipadeola AK, Naidoo SR, Quandt A, Ozoemena KI: **Annealing boosts the supercapacitive properties of molybdenum disulfide powder**. *Electroanalysis* 2020, **32**:2642–2649.

18. Ipadeola AK, Mwonga PV, Ray SC, Maphanga RR, Ozoemena KI: **Palladium/stannic oxide interfacial chemistry promotes hydrogen oxidation reactions in alkaline medium**. *Chemelectrochem* 2020, **7**:4562–4571.

19. Ipadeola AK, Ozoemena KI: **Alkaline water-splitting reactions over Pd/Co-MOF-derived carbon obtained via microwave-assisted synthesis**. *RSC Adv* 2020, **10**:17359–17368.

20. Mofokeng TP, Ipadeola AK, Tetana ZN, Ozoemena KI: **Defect-engineered nanostructured Ni/MOF-derived carbons for an efficient aqueous battery-type energy storage device**. *ACS Omega* 2020, **5**:20461–20472.

21. Liu Y, Yang L, Xie B, Zhao N, Yang L, Zhan F, Pan Q, Han J, Wang X, Liu J, Li J, Yang Y: **Ultrathin Co_3O_4 nanosheet clusters anchored on nitrogen doped carbon nanotubes/3D graphene as binder-free cathodes for Al-air battery**. *Chem Eng J* 2020, **381**, 122681.

22. Liu Y, Zhan F, Zhao N, Pan Q, Li Z, Du Y, Yang Y: **Reduced mesoporous Co3O4 nanowires grown on 3D graphene as efficient catalysts for oxygen reduction and binder-free electrodes in aluminum–air batteries**. *J Mater Sci* 2021, **56**:3861–3873.

23. Wang Z, Zhou H, Xue J, Liu X, Liu S, Li X, He D: **Ultrasonic-assisted hydrothermal synthesis of cobalt oxide/nitrogen-doped graphene oxide hybrid as oxygen reduction reaction catalyst for Al-air battery**. *Ultrason Sonochem* 2021, **72**, 105457.

24. Liu S, Cao Z, Meng Y, Li Y, Yang W, Chang Z, Liu W, Sun X: **Aerophilic Co-embedded N-doped carbon nanotube arrays as highly efficient cathodes for aluminum–air batteries**. *ACS Appl Mater Interfaces* 2021, **13**:26853–26860.

25. Sun S, Zhang Z, Yan L, Li C, Li H, Qiao Z, Yu Z, Li W, Wang N, Jiang Y: **A novel superimposed porous copper/carbon film derived from polymer matrix as catalyst support for metal-air battery**. *J Porous Mater* 2022, **29**:249–255.

26. Li J, Kang L, Luo K, Huang Y, Zhong S, Yan D: **Encapsulating Cu_2Se into 3D porous carbon as high-voltage electrode materials for aluminum-ion batteries**. *Ceram Int* 2023, **49**:2613–2618.

27. ** Fu X, Jiang G, Wen G, Gao R, Li S, Li M, Zhu J, Zheng Y, Li Z, Hu Y, Yang L, Bai Z, Yu A, Chen Z: **Densely accessible Fe-N_x active sites decorated mesoporous-carbon-spheres for oxygen reduction towards high performance aluminum-air flow batteries**. *Appl Catal B* 2021, **293**, 120176.

This study utilized a facile dual-template approach to fabricate single-atomic Fe-N_x moieties coupled mesoporous carbon spheres, with 2D-porous-air-cathode that boosted O2 transfer and abundant active-sites in AAB, resulting in excellent gravimetric energy density and discharging stability.

28. * Huang L, Zang W, Ma Y, Zhu C, Cai D, Chen H, Zhang J, Yu H, Zou Q, Wu L, Guan C: **In-situ formation of isolated iron sites coordinated on nitrogen-doped carbon coated carbon cloth as self-supporting electrode for flexible aluminum-air battery**. *Chem Eng J* 2021, **421**, 129973.

In this work, a self-supporting air-cathode, containing isolated Fe-single-atoms on NC, was in situ fabricated from templates (ferrocene and Zn-MOF) on CC, and showed promising performance in flexible AAB.

29. Luo Y, Chen Y, Xue Y, Chen J, Wang G, Wang R, Yu M, Zhang J: **Electronic structure regulation of iron phthalocyanine induced by anchoring on heteroatom-doping carbon sphere for efficient oxygen reduction reaction and Al–air battery**. *Small* 2022, **18**, 2105594.

30. Katsoufis P, Katsaiti M, Mourelas C, Andrade TS, Dracopoulos V, Politis C, Avgouropoulos G, Lianos P: **Study of a thin film aluminum-air battery**. *Energies* 2020, **13**:1447.

31. Ma J, Zhang Y, Qin C, Ren F, Wang G: **Effects of polystyrene sulfonate/graphene and Mn3O4/graphene on property of aluminum(zinc)-air batteries**. *Int J Hydrogen Energy* 2020, **45**:13025–13034.

32. Shui Z, Liao X, Lei Y, Ni J, Liu Y, Dan Y, Zhao W, Chen X: **MnO2 synergized with N/S codoped graphene as a flexible cathode efficient electrocatalyst for advanced honeycomb-shaped stretchable aluminum–air batteries**. *Langmuir* 2020, **36**:12954–12962.

33. Huo G, Wang X-W, Zhang Z-B, Song Z, Kang X-M, Chen M-X, Wang Q, Fu X-Z, Luo J-L: **γ-MnO_2 nanorod-assembled hierarchical micro-spheres with oxygen vacancies to enhance electrocatalytic performance toward the oxygen reduction reaction for aluminum-air batteries**. *J Energy Chem* 2020, **51**:81–89.

34. Cheng R, Wang F, Jiang M, Li K, Zhao T, Meng P, Yang J, Fu C: **Plasma-assisted synthesis of defect-rich O and N codoped carbon nanofibers loaded with manganese oxides as an efficient oxygen reduction electrocatalyst for aluminum–air batteries**. *ACS Appl Mater Interfaces* 2021, **13**:37123–37132.

35. Mphahlele NE, Ipadeola AK, Haruna AB, Mwonga PV, Modibedi RM, Palaniyandy N, Billing C, Ozoemena KI: **Microwave-induced defective PdFe/C nano-electrocatalyst for highly efficient alkaline glycerol oxidation reactions**. *Electrochim Acta* 2022, **409**, 139977.

36. Ipadeola AK, Eid K, Lebechi AK, Abdullah AM, Ozoemena KI: **Porous multi-metallic Pt-based nanostructures as efficient electrocatalysts for ethanol oxidation: strategy and mechanism**. *Electrochem Commun* 2022, **140**, 107330.

37. Xia Z, Zhu Y, Zhang W, Hu T, Chen T, Zhang J, Liu Y, Ma H, Fang H, Li L: **Cobalt ion intercalated MnO2/C as air cathode catalyst for rechargeable aluminum–air battery**. *J Alloys Compd* 2020, **824**, 153950.

38. Hu T, Zhang W, Xia Z, Zhu Y, Liu Y, Zhang J, Li L: **Growth restriction of Co3O4 nanoparticles by α-MnO_2 nanorods as air cathode catalyst for rechargeable aluminum-air battery**. *Int J Energy Res* 2022, **46**:11174–11184.

39. ** Deng J, Lu H, Xu B, Cao Y, Yang W, Liu J: **$NiMn_2O_4$-based Ni-Mn bimetallic oxides as electrocatalysts for the oxygen reduction reaction in Al–air batteries**. *Chem Eng J* 2021, **413**, 127439.

The fabrication of Ni–Mn bimetallic oxides as air-cathode was achieved by simple preparation with tailored nanorods morpholog for AAB, where optimized atomic ratio of the metals (Mn^{3+}+Mn^{4+})/Mn^{2+} and (Ni^{3+}/Ni^{2+}) is beneficial for a high specific capacity.

40. ** Liu D, Tian J, Tang Y, Li J, Yi S, Huang X, Sun D, Wang H: **High-power double-face flow Al-air battery enabled by CeO2 decorated MnOOH nanorods catalyst**. *Chem Eng J* 2021, **406**, 126772.

In this work, the promotion effect of CeO_2 on MnOOH nanorods was studied as air-cathode in a double-face flow AAB for practical

applications, which had great power density, specific capacity and energy density than those of 20%Pt/C.

41. Guo M, Zhang X, Yang T, Dang Q, Li X, Wang Y, Zhang G: **Binary FeCo-N-doped carbon/carbon nanotube composites for efficient oxygen reduction and high-performance aluminum-air battery**. *J Power Sources* 2020, **456**, 227933.

42. Lu M, An L, Yin J, Jin J, Yang R, Huang B, Hu Y, Zhao Y-Q, Xi P: **Electronic engineering of amorphous Fe−Co−S sites in hetero-nanoframes for oxygen evolution and flexible Al−air batteries**. *J Mater Chem* 2022, **10**:19757−19768.

43. Jiang M, Yang J, Ju J, Zhang W, He L, Zhang J, Fu C, Sun B: **Space-confined synthesis of CoNi nanoalloy in N-doped porous carbon frameworks as efficient oxygen reduction catalyst for neutral and alkaline aluminum-air batteries**. *Energy Storage Mater* 2020, **27**:96−108.

44. Tian W-W, Ren J-T, Yuan Z-Y: **In-situ cobalt-nickel alloy catalyzed nitrogen-doped carbon nanotube arrays as superior freestanding air electrodes for flexible zinc-air and aluminum-air batteries**. *Appl Catal B* 2022, **317**, 121764.

45. Kang R, Du Y, Zhou W, Zhang D, Zhang W, Wan J, Chen G, Zhang J: **Synthesis design of bimetallic selenide $NiCoSe_2$@ F-doped C with core−shell structure as cathode for advanced rechargeable aluminum batteries**. *ACS Appl Energy Mater* 2022, **5**:10287−10296.

46. * Jiang M, Fu C, Cheng R, Liu T, Guo M, Meng P, Zhang J, Sun B: **Interface engineering of Co3Fe7-Fe3C heterostructure as an efficient oxygen reduction reaction electrocatalyst for aluminum-air batteries**. *Chem Eng J* 2021, **404**, 127124.
This study strategically engineered multifunctional air-cathode with interfacial heterostructure and honeycomb-like morphology, which displayed promising performance in AAB with high open-circuit voltage and power density.

47. ** Jiang M, Fu C, Cheng R, Zhang W, Liu T, Wang R, Zhang J, Sun B: **Integrated and binder-free air cathodes of Co3Fe7 nanoalloy and Co5.47N encapsulated in nitrogen-doped carbon foam with superior oxygen reduction activity in flexible aluminum-air batteries**. *Adv Sci* 2020, **7**, 2000747.
This study developed an integrated and additive-free air-cathode, consisting of a free -standing Co_3Fe_7 nanoalloy and $Co_{5.47}N$ embebbed N-dope carbon foam (Co_3Fe_7@$Co_{5.47}$N/NCF) for flexible aluminium-air battery with impressive performance, which was superiot to slurry casting air-cathode.

48. Yu D, Ma Y, Hu F, Lin C-C, Li L, Chen H-Y, Han X, Peng S: **Dual-sites coordination engineering of single atom catalysts for flexible metal−air batteries**. *Adv Energy Mater* 2021, **11**, 2101242.

49. Lu H, Li Y, Zheng Y, Dong C, Li Y, Meng F, Wang Y, Teng C, Wang X, Zhou D: **Layered double hydroxide-derived Fe-doped NiSe cathode toward stable and high-energy aluminum storage**. *Mater Today Energy* 2022, **24**, 100940.

50. Chen W, Yu H, Chang S, Li W, Liu R, Wang Y, Zhang H, Zhang Z: **Wheat straw as carbon source to prepare $FeCoP_2$/N, P Dual-Doped carbon matrix as bifunctional catalyst for application in rechargeable Zinc-air and Aluminum-air batteries**. *Appl Surf Sci* 2022, **573**, 151486.

51. * He T, Chen Y, Liu Q, Lu B, Song X, Liu H, Liu M, Liu Y-N, Zhang Y, Ouyang X, Chen S: **Theory-guided regulation of FeN4 spin state by neighboring Cu atoms for enhanced oxygen reduction electrocatalysis in flexible metal−air batteries**. *Angew Chem Int Ed* 2022, **61**:e202201007.
In this work, theoretical simulations of coupling Cu atoms with FeN_4 spin-state tuned its energy barrier and magnetic moment for excellent air-cathode performance with impressive open-circuit voltage and power density.

52. Shui Z, Zhao W, Xiao H, Zhu L, Liu Y, Deng X, Chen X: **Controllable porous perovskite with three-dimensional ordered structure as an efficient oxygen reduction reaction electrocatalyst for flexible aluminum-air battery**. *J Power Sources* 2022, **523**, 231028.

53. Ipadeola AK, Lebechi AK, Gaolatlhe L, Haruna AB, Chitt M, Eid K, Abdullah AM, Ozoemena KI: **Porous high-entropy alloys as efficient electrocatalysts for water-splitting reactions**. *Electrochem Commun* 2022, **136**, 107207.

54. Shui Ziyi HN, Chen Li, Zhao Wei, Chen Xi: **Porous perovskite towards oxygen reduction reaction in flexible aluminum-air battery**. *Acta Chim. Sin.* 2020, **78**:557−564.

55. Yu L, Xu N, Zhu T, Xu Z, Sun M, Geng D: **La0.4Sr0.6Co0.7-Fe0.2Nb0.1O3-δ perovskite prepared by the sol-gel method with superior performance as a bifunctional oxygen electrocatalyst**. *Int J Hydrogen Energy* 2020, **45**:30583−30591.